GLIA

WILEY

RESEARCH ARTICLE

The laminar position, morphology, and gene expression profiles of cortical astrocytes are influenced by time of birth from ventricular/subventricular progenitors

Daniela Lozano Casasbuenas[1,2] | Ines Kortebi[1,3] | Charles Gora[4] | Erica Y. Scott[1,5,6] | Celeste Gomes[1] | Markley Silva Oliveira Jr[7] | Tanvi Sharma[1] | Emerson Daniele[1,3] | Arman Olfat[1] | Rachel Gibbs[1,3] | Scott A. Yuzwa[2] | Emily A. Gilbert[1] | Patrick Küry[7,8] | Aaron R. Wheeler[5,6,9] | Martin Lévesque[4] | Maryam Faiz[1,2,3]

[1]Division of Anatomy, Department of Surgery, University of Toronto, Toronto, Ontario, Canada

[2]Department of Laboratory Medicine and Pathobiology, University of Toronto, Toronto, Ontario, Canada

[3]Institute of Medical Science, University of Toronto, Toronto, Ontario, Canada

[4]Department of Psychiatry and Neurosciences, Université Laval, Québec, Canada; CERVO Brain Research Center, Québec, Canada

[5]Department of Chemistry, University of Toronto, Toronto, Ontario, Canada

[6]Donnelly Centre for Cellular and Biomolecular Research, University of Toronto, Toronto, Ontario, Canada

[7]Neuroregeneration Laboratory, Department of Neurology, Medical Faculty, Heinrich-Heine University, Düsseldorf, Germany

[8]Department of Neurology, Inselspital, Bern University Hospital and University of Bern, Bern, Switzerland

[9]Institute of Biomedical Engineering, University of Toronto, Toronto, Ontario, Canada

Correspondence

Maryam Faiz, Division of Anatomy, Department of Surgery, University of Toronto, Toronto, Ontario, Canada.
Email: maryam.faiz@utoronto.ca

Abstract

Astrocytes that reside in superficial (SL) and deep cortical layers have distinct molecular profiles and morphologies, which may underlie specific functions. Here, we demonstrate that the production of SL and deep layer (DL) astrocyte populations from neural progenitor cells in the mouse is temporally regulated. Lineage tracking following *in utero* and postnatal electroporation with *PiggyBac* (*PB*) EGFP and birth dating with EdU and FlashTag, showed that apical progenitors produce astrocytes during late embryogenesis (E16.5) that are biased to the SL, while postnatally labeled (P0) astrocytes are biased to the DL. In contrast, astrocytes born during the predominantly neurogenic window (E14.5) showed a random distribution in the SL and DL. Of interest, E13.5 astrocytes birth dated at E13.5 with EdU showed a lower layer bias, while FT labeling of apical progenitors showed no bias. Finally, examination of the morphologies of "biased" E16.5- and P0-labeled astrocytes demonstrated that E16.5-labeled astrocytes exhibit different morphologies in different layers, while P0-labeled astrocytes do not.

Daniela Lozano Casasbuenas and Ines Kortebi equally contributed as first authors.

Differences based on time of birth are also observed in the molecular profiles of E16.5 versus P0-labeled astrocytes. Altogether, these results suggest that the morphological, molecular, and positional diversity of cortical astrocytes is related to their time of birth from ventricular/subventricular zone progenitors.

KEYWORDS

astrocyte, cortical development, neural progenitor cell, radial glia, ventricular/subventricular zone

1 | INTRODUCTION

During cortical development, progenitor cells in the ventricular/subventricular zone (VZ/SVZ) give rise to neurons, astrocytes, and oligodendrocytes (Miller & Gauthier, 2007). It is well known that the temporal and spatial patterning of apical progenitors (radial glia) contributes to the production of diverse projection neurons with distinct molecular and anatomical profiles (Guillemot, 2007). Deep layer (DL) neurons are born first (E11.5–E13.5) and mainly project to subcortical regions, while superficial layer (SL) neurons are born later (E14.5–E16.5) and mainly project intracortically (Molyneaux et al., 2007). Following the production of cortical neurons, these VZ/SVZ progenitors "switch" to astrocyte production (Miller & Gauthier, 2007).

Astrocytes are first detected in the developing cortex around E16.5 (Bayraktar et al., 2014) and have fully colonized the cortex by P21 (Clavreul et al., 2019). During late embryogenesis, astrocyte progenitors are produced directly from translocating apical progenitors (Noctor et al., 2008) and indirectly via multipotent progenitor cells (Li et al., 2021). After birth, a second wave of astrocyte progenitors arises from basal multipotent intermediate progenitor cells (Li et al., 2021). It has also been demonstrated that both NG2+ progenitors (Huang et al., 2014; Sanchez-Gonzalez et al., 2020) and migratory subpallial progenitors (Marshall & Goldman, 2002; Nery et al., 2002) give rise to cortical astrocytes. In the early postnatal period (P3–P7), astrocytes proliferate and disperse to colonize the cortex (Clavreul et al., 2019; Ge et al., 2012). By P7, they have assumed their final locations and undergo maturation until P21 (Clavreul et al., 2019).

Recent studies of the spinal cord and cerebellum suggest that progenitor patterning may also influence astrocyte identity (Cerrato et al., 2018; Garcia-Marques & Lopez-Mascaraque, 2013; Hochstim et al., 2008; Magavi et al., 2012; Tsai et al., 2012). In the spinal cord, astrocytes in different regions are produced according to the precise expression of transcription factors in radial glia (Hochstim et al., 2008; Tsai et al., 2012). Similarly, in the cerebellum, clonal analysis shows that spatiotemporal patterning determines the production of distinct cerebellar astrocyte types (Cerrato et al., 2018).

In the cortex, astrocytes in different layers and regions have distinct morphologies and gene expression signatures (Bayraktar et al., 2018; Lanjakornsiripan et al., 2018; Morel et al., 2017); whether this organization results from progenitor patterning is not entirely clear. Several studies have suggested that the production of astrocytes from progenitors is spatially restricted; clonal Cre/Lox-based fate mapping shows that

astrocytes are associated with cortical columns, and mapping of astrocytes produced from radial glia shows their distribution according to the processes of radial glial cells (Magavi et al., 2012). In addition, Star Track clonal labeling has suggested that cortical progenitors are heterogeneous with respect to the types of astrocytes they produce (Garcia-Marques & Lopez-Mascaraque, 2013; Ojalvo-Sanz & Lopez-Mascaraque, 2021; Sanchez-Gonzalez et al., 2020). Conversely, multi addressable genome-integrative color marker-based mapping points to an alternate model in which astrocytes occupy the cortex in a disorganized manner largely based on local cues (Clavreul et al., 2019). However, one limitation of these studies was that progenitors were labeled at a single time point during development (Clavreul et al., 2019; Garcia-Marques & Lopez-Mascaraque, 2013; Ojalvo-Sanz & Lopez-Mascaraque, 2021), so these analyses reflect the cumulative production of astrocytes over time. Thus, further work is needed to understand how time influences cortical astrocyte diversity.

Here, we asked whether the time of birth from VZ/SVZ progenitors influences the laminar distribution, morphology, and molecular profiles of astrocytes in the cerebral cortex. We labeled progenitors at different times using three orthogonal fate mapping strategies: in utero electroporation, EdU fate-mapping, and FlashTag (FT) birth dating. We found that astrocytes born from progenitors during late embryogenesis (E16.5) show an upper layer bias while postnatally born (P0) astrocytes show a lower layer bias. In contrast, astrocytes labeled at E14.5 show no bias using all three strategies, while E13.5 labeled progenitors only show a bias with EdU fate mapping. We then examined the morphologies and molecular profiles of E16.5- and P0-labeled astrocytes in different cortical layers. We found that E16.5-born astrocytes show layer-based morphological differences, while P0-born astrocytes do not. Similarly, transcriptomic analysis of E16.5- and P0-labeled cells show that their molecular profiles are influenced by time of birth. Our findings suggest that temporal patterning in VZ/SVZ progenitors is important for the laminar diversity of cortical astrocytes.

2 | METHODS

2.1 | Mice

CD-1® IGS timed pregnant females purchased from Charles River were used in all experiments. Females were housed individually with their litters in the animal vivarium with standard 12 h:12 h light/dark cycle and ad libitum access to rodent chow and water. Cages were

also provided with sunflower seeds and water bottles. Both female and male embryos and pups were used for experiments. All experiments were conducted according to protocols approved by the animal care committees at the Department of Comparative Medicine at the University of Toronto (AUP #20001954) and the Toronto Center for Phenogenomics (AUP#25-0388H).

2.2 | Plasmids

All plasmids were purchased as *Escherichia coli* stocks from Vector Builder (*PB*-CAG::EGFP: VB900088-2260upr, *PB*-CAG::CreERT2: VB190625-1140skh, *PB*-LSL-CAG::EGFP: VB210420-1195qzx, *PB*-LSL-CAG::mCherry: VB170516-1125bjp) and amplified using the PureLink™ HiPure Plasmid Filter Maxiprep Kit (K210017, Invitrogen).

2.3 | Electroporation

2.3.1 | In utero electroporation

Timed pregnant CD1 mice were anesthetized with isoflurane (induction: 5%; surgery: 2%–3%). Analgesia (Ketoprofen, 5 mg/kg; Buprenorphine 1 mg/kg) and 1 mL Ringer's Lactate was administered subcutaneously. The abdomen was shaved and disinfected using 70% ethanol and povidone-iodine. The female was placed on a heating pad set to 37°C. Prior to abdominal incision, a lack of a pedal reflex was observed. The uterine horns were then exposed by laparotomy and soaked every 2 min with sterile phosphate-buffered saline (PBS). One microliter of DNA (1 μg/μL in water, 1:5 *PB*-hyperbase [a gift from A. Nagy] to *PB*-CAG::EGFP ratio) mixed with Trypan Blue (15250061, Gibco, 1 μL per 10 μL of plasmid solution) was injected through the uterine wall into one of the embryonic lateral ventricles using a pulled glass pipette (1-000-0500, Microcaps). The embryos lining the birth canal were omitted to prevent blockage of the canal during labor in the event of non-survival. Each embryo head was carefully placed between 5 mm circular electrodes (Platinum Tweezertrodes, BTX) presoaked in PBS. Electrodes were oriented to target the dorsal V/SVZ. Five electrical pulses were delivered using a square-wave electroporation generator (ECM 830, BTX) using the following settings: amplitude 40 V, duration 50 ms, intervals 950 ms. After electroporation, the uterine horns were returned into the abdominal cavity and the peritoneum was sutured. Ringer's lactate solution was then injected into the peritoneum to float the internal organs and help reposition them. Following suturing of the skin, the female was left to recover under a heating lamp before being moved into the home cage. The embryos were left to continue their normal development until sacrifice.

2.3.2 | Postnatal electroporation

P0 pups were anesthetized using isoflurane (2%–3%). Pups were injected with 2 μL of DNA (5 μg/μL in water, 1:5 PB-hyperbase to X

fluorescent protein (XFP) ratio, PB-CAG::CreERT2 with PB-CAG-LSL::EGFP or PB-LSL-CAG::mCherry) mixed with Trypan Blue (1 μL per 10 μL plasmid solution) using a pulled glass pipette needle (1-000-0500, Microcaps). Each pup head was carefully placed between 5 mm circular electrodes presoaked in PBS. Electrodes were oriented to target the dorsal SVZ. Five electrical pulses were delivered to each pup with the following settings: amplitude 100 V, duration 50 ms, intervals 950 ms. Pups were returned to their mother.

2.4 | Tamoxifen induction

Tamoxifen solution was prepared fresh before each injection. Fifteen milligrams of tamoxifen (T5648, Sigma-Aldrich) was dissolved in 100 μL 100% ethanol and 900 μL sunflower seed oil (S5007, Sigma-Aldrich). The solution was heated at 95°C for 1 min. Pregnant and lactating females with P0 litters were injected with 3 mg of tamoxifen (0.2 mL solution) intraperitoneally once daily for three consecutive days (P1–P3, P3–P5, or P5–P7).

2.5 | EdU injections

EdU solution was prepared as per the instructions in the Click-iT™ EdU Cell Proliferation Kit (Alexa Fluor™ 647, C10340, Invitrogen). A single injection of 0.25 mg EdU in 100 μL of PBS was administered intraperitoneally to pregnant dams.

2.6 | FT injections

2.6.1 | FT working solution

FT was prepared by diluting 50 μg Carboxyfluorescein succinimidyl ester (CFSE; CellTrace™ CFSE Cell Proliferation Kit (Component A), C34554, Invitrogen] in 9 μL DMSO (CellTrace™ CFSE Cell Proliferation Kit (Component B), C34554, Invitrogen) followed by adding 1.8 μL (Trypan Blue, 15250061, Gibco) and 7.2 μL sterile water for a final concentration of 5 mM CFSE.

2.6.2 | In utero FT injections

All surgical in utero procedures were performed as stated above. In brief, timed pregnant CD1 mice were anesthetized with isoflurane; analgesia and Ringer's lactate were administered subcutaneously. The uterine horns were then exposed by laparotomy. One microliter of the FT working solution was injected through the uterine wall into one of the lateral ventricles of the embryos using a pulled glass pipette (1-000-0500, Microcaps). The uterine horns were returned into the abdominal cavity and the embryos were left to continue their normal development until sacrifice.

2.7 | Immunohistochemistry

At P3, tissue was postfixed in 4% PFA for 24 h before being transferred to 30% sucrose solution for cryoprotection. At P21, animals were sacrificed by transcardial perfusion of 15 mL PBS followed by 15 mL 4% PFA solution in PBS (pH = 7.4), then postfixed for 24 h in 4% PFA. Following fixation, tissue was cryoprotected in a 30% sucrose solution overnight. Brains were sectioned at 20 μM on a cryostat (HM525 NX, Thermo Fisher) and mounted on Superfrost™ Plus slides (12-550-15, Fisher Scientific).

Slides were washed 3 times for 5 min in PBS prior to permeabilization blocking (0.3% Triton X-100, 5% bovine serum albumin [BSA, ALB001, BioShop], 10% normal goat serum [NGS, 005-000-121, Jackson Immuno Research] in PBS) for 1 h at RT in a humid chamber. Primary antibodies (Table 1) were diluted in the blocking solution and incubated overnight in a humid chamber at 4°C. Slides were washed 3 times for 5 min in PBS before adding secondary antibodies. Secondary antibodies (Table 1) were diluted in blocking solution and incubated at RT for 1 h in a humid chamber. Slides were washed three times with PBS for 5 min, then incubated at RT in 1:3000 4′,6-diamidino-2-phenylindole (DAPI) in PBS for 5 min. Slides were washed for 5 min in distilled water before mounting using Mowiol. For sections containing EdU, slides were washed 3 times in PBS and incubated in 4% PFA for 20 min after secondary antibody incubation. The Click-iT™ EdU Cell Proliferation Kit was used to stain EdU+ cells, followed by PBS washes, DAPI incubation, and a distilled water rinse before mounting.

2.8 | Imaging and cell counts

Tiled images of the cortex were captured using a Zeiss LSM 880 super resolution confocal. Three sections per animal were used for cell counting. SL (layers 2–4) and DL (layers 5/6) were distinguished based on dense layer IV DAPI staining. All cell counts were performed in three sections per animal.

2.9 | Tissue clearing and morphology analysis

Fixed brain tissues were sliced at 250 μm thickness using a vibratome prior clarification. Tissue clearing was performed using a tissue clearing kit (HRTC-012, Binaree) with the following modifications. Sections were incubated in 35% sucrose overnight, followed by 2 h in 500 mL

of solution A. Sections were then washed in 1× PBS four times for 20 min. Finally, sections were incubated in 600 mL for 2 h in the mounting solution (HRMP-006, Binaree) and stored at room temperature until imaging. Z-stacks of EGFP+ astrocytes from cleared sections were acquired using a Zeiss LSM710 confocal microscope with a 20× objective for an optimal working distance from the sample.

Confocal images were processed with the Fiji Package of ImageJ. For morphology analysis, 3D objects of individual EGFP+ astrocytes were extracted with the 3D Object Counter Plugin of Fiji based on the green channel (EGFP) (video S1). The 3D objects were then analyzed using the 3D Suite Plugin for (Ollion et al., 2013) to measure territorial volume, surface area, compactness, sphericity, Feret, ellipsoid, major radius, ellipsoid elongation, ellipsoid flatness, and volume ratio (ellipsoid/object).

All 11 morphological features outlined above, were compiled for 453 cells with birth time and layer metadata appended. These values for each feature were converted into z-scores (scaled) to account for different units between features. The scaled features were hierarchically clustered (Ward algorithm) and plotted on a dendrogram in R using R packages ggdendro, dendextend, and ggplot2.

2.10 | TissueDISCO-based transcriptomics

Electroporated tissue was mounted onto tDISCO slides as previously described (Scott et al., 2024). Tissue was then fixed with 4%PFA for 20 min at room temperature. Tissue was permeabilized for 15 min at room temperature (0.3% Triton X-100), blocked for 1 h (0.1% Triton, 0.075% BSA), and stained with anti-SOX9 (rabbit, 1:200, Millipore AB5535) and chicken-anti-GFP (1:200, Aves GFP-1020) and Alexa-Fluor 488 and 568 (1:200, Invitrogen A11034 & A11036). Individual cells were isolated using laser-induced cavitation bubbles and collected using digital microfluidics in a 3 μL volume, as previously described (Scott et al., 2024). Cell lysates were incubated at 50°C for 30 min to reverse PFA-induced cross-linking and then brought through regular reverse transcription and Nextera XT prep as previously described (Scott et al., 2024). All data were demultiplexed and mapped using previous scripts. EdgeR was used to perform differential gene expression (DEG) analysis between E16.5-birthed and P0-birthed using general linear models and contrasts. All scripts can be found at github.com/eyscott/Astrocyte_Dev.

2.11 | Statistical analysis

Data are show as mean + standard error of the mean (SEM). Graph-Pad Prism version 9.1.0 for Mac (GraphPad Software, San Diego, California USA, www.graphpad.com) was used to perform all statistical analyses and create graphs. For cell quantification of electroporation, EdU and FT experiments, proportions were transformed using the arcsine function. To assess Gaussian distribution, the Shapiro Wilk normality test was used for all datasets. SL vs. DL data were compared within a time point using paired t-tests. For FT layer counts and

TABLE 1 Primary and secondary antibodies.

Antibody (host)	Company	Dilution
Anti-NeuN (rabbit)	Millipore, ABN78	1:200
Anti-SOX9 (rabbit)	Millipore, AB5535	1:200
Anit-ALDH1L1 (rabbit)	Abcam, AB87117	1:200
Alexa Fluor™ 568 (goat anti-rabbit, IgG)	Invitrogen, A-11036	1:400

morphology analysis, a one-way analysis of variance (ANOVA) with a Tukey's post hoc test for multiple comparisons was used. All experiments were performed from pups across at least two litters.

3 | RESULTS

3.1 | *PiggyBac* fate mapping shows that pallial progenitors labeled during late embryogenesis produce mostly SL astrocytes, while postnatal progenitors produce DL astrocytes

To determine whether astrocyte production is temporally regulated, pallial VZ/SVZ progenitors were electroporated with *PiggyBac* (*PB*)-CAG::EGFP at three different time points during development: (i) E14.5 during a period of predominant neurogenesis, (ii) E16.5 during late embryogenesis, and (iii) P0, after birth (Figure 1a). At P21, we were able to detect EGFP+ VZ/SVZ progenitor cells (Figure S1) and, similar to previous reports (Tabata & Nakajima, 2001), EGFP+ cells with a bushy morphology typical of astrocytes dispersed throughout the cortex (Figure 1b–d). To examine the distribution of astrocytes labeled at different time points in the superficial (Layers 2–4; SL) or deep (Layers 5–6; DL), we quantified the number of EGFP+ cells that expressed astrocyte lineage markers, SOX9, and ALDHL1L1 in each region at P21. We found that E14.5-labeled progenitors gave rise to SOX9+EGFP+ and ALDH1L1+ EGFP+ astrocytes that were equally distributed in the SL or DL at P21 (Figure 1b,e, Figure S2a). However, when we examined E16.5- and P0-labeled astrocytes, we found that E16.5-labeled SOX9+EGFP+ and ALD1H1L1+EGFP+ astrocytes showed a biased distribution in the SL (Figure 1c,f, Figure S2a). In contrast, P0-labeled SOX9+EGFP+ and ALD1H1L1+EGFP+ showed a DL bias (Figure 1d, g, Figure S2a). To understand whether a biased distribution of SL astrocytes was present throughout late embryogenesis or limited to E16.5-labeled astrocytes, we electroporated VZ/SVZ progenitors with *PB*-CAG::EGFP at E15.5 and E17.5. We found that E15.5 and E17.5-labeled SOX9+EGFP astrocytes also showed a biased distribution in the SL (Figure S2b), suggesting that VZ/SVZ progenitors produce astrocytes that mainly occupy the SL throughout late embryogenesis.

We also examined whether a DL-astrocyte bias existed throughout the early postnatal period. We electroporated P0 progenitors with *PB*-CAG::CreERT2 and *PB*-CAG::LSL-EXFP and then induced XFP labeling in progenitors with tamoxifen administration during three different time windows, P1–P3, P3–P5, and P5–P7. Labeling of progenitors within each of these postnatal windows also showed a DL bias in astrocytes, suggesting that astrocytes produced during early postnatal cortical development are mainly distributed in the DL (Figure S2c).

3.1.1 | EdU fate mapping confirms a time-dependent layer bias

To confirm the layer bias we had observed in astrocytes produced during embryogenesis, we used a well-established EdU fate-mapping approach (Hofer et al., 2016). We labeled dividing cells with EdU at E14.5 and E16.5 and quantified EdU+SOX9+ astrocytes at P3 or P21. We did not detect any E14.5 or E16.5-labeled EdU+SOX9+ astrocytes at P21 (Figure S3a,b), in line with previous studies that suggest astrocytes undergo a period of massive expansion between P3 and P7 to colonize the cortex (Clavreul et al., 2019; Ge et al., 2012).

At P3, EdU fate mapping showed an SL bias in EdU+SOX9+ astrocytes labeled at E16.5 (Figure 2a,d,e), consistent with our PB-CAG-EGFP labeling paradigm (Figure 1f). However, when we examined E14.5-labeled cortices, no EdU+SOX9+ cells were found (Figure S3c–e). We hypothesized that the lack of EdU label retention in SOX9+ astrocytes at P3 was due to fast division within their parent progenitor pool. To test this hypothesis, we sacrificed E14.5 labeled embryos at E18.5. At E18.5, we were able to detect EdU+SOX9+ cells. These EdU+SOX9+ cells showed no bias in their distribution within the SL or DL (Figure 2b,f,g), consistent with our previous findings (Figure 1e).

From E12.5 to E14.5, VZ/SVZ progenitors go through multiple transitions. They switch their mode of division from symmetric to primarily asymmetric (Gao et al., 2014); some of these cells become "slow-dividing" to enable the emergence of adult NSCs in the VZ/SVZ (Fuentealba et al., 2015; Furutachi et al., 2015). Therefore, we asked how astrocytes would disperse in the cortex after labeling E13.5 progenitors. To our surprise, unlike E14.5-labeled cells that did not show a layer bias, E13.5-labeled astrocytes showed a biased distribution in the DL at P3 (Figure 2c,h,i). Our E13.5 findings suggested again that temporal patterning of progenitors influences cortical astrocyte distribution.

3.1.2 | FT fate mapping shows a layer bias in cortical astrocytes that depends on the time of birth from apical VZ/SVZ progenitors

EdU fate mapping could not distinguish between VZ/SVZ-derived astrocytes and those born from other progenitor pools that are also known to contribute to cortical astrocyte formation (Bandler et al., 2022; Marshall & Goldman, 2002; Nery et al., 2002). To understand whether these layer biases were present in the astrocyte progeny of apical VZ/SVZ progenitors, we used the FT fate-mapping approach. FT labels the M-phase of apical VZ/SVZ progenitors and their progeny within a two-hour window (Govindan et al., 2018; Oberst et al., 2019). We labeled apical progenitors with FT at E13.5, E16.5, or P0 (Figure 3a, Figure S4), time points where we observed a layer-biased distribution of astrocytes and quantified FT+SOX9+ within the SL and DL at P3. We found that apical E16.5-labeled progenitors produced FT+SOX9+ astrocytes that showed a biased location in the SL, while P0-labeled progenitors produced FT+SOX9+ astrocytes that mainly occupied the DL (Figure S4a,b). Astrocytes labeled at E13.5 showed no bias (Figure S4c,d), in contrast to our EdU fate mapping results (Figure 2i). This finding may suggest that E13.5-labeled astrocytes are derived from a different progenitor source (Marshall & Goldman, 2002; Nery et al., 2002).

To further resolve the spatial localization of E16.5- and P0-FT+ astrocytes, we quantified the number of E16.5- and P0- born FT+SOX9+ cells within each cortical layer. We found that E16.5-born FT+SOX9+ astrocytes were biased to layers 2/3 (Figure 3b,c), while P0-born FT+SOX9+ astrocytes were mostly found in layer 6 (Figure 3d,e).
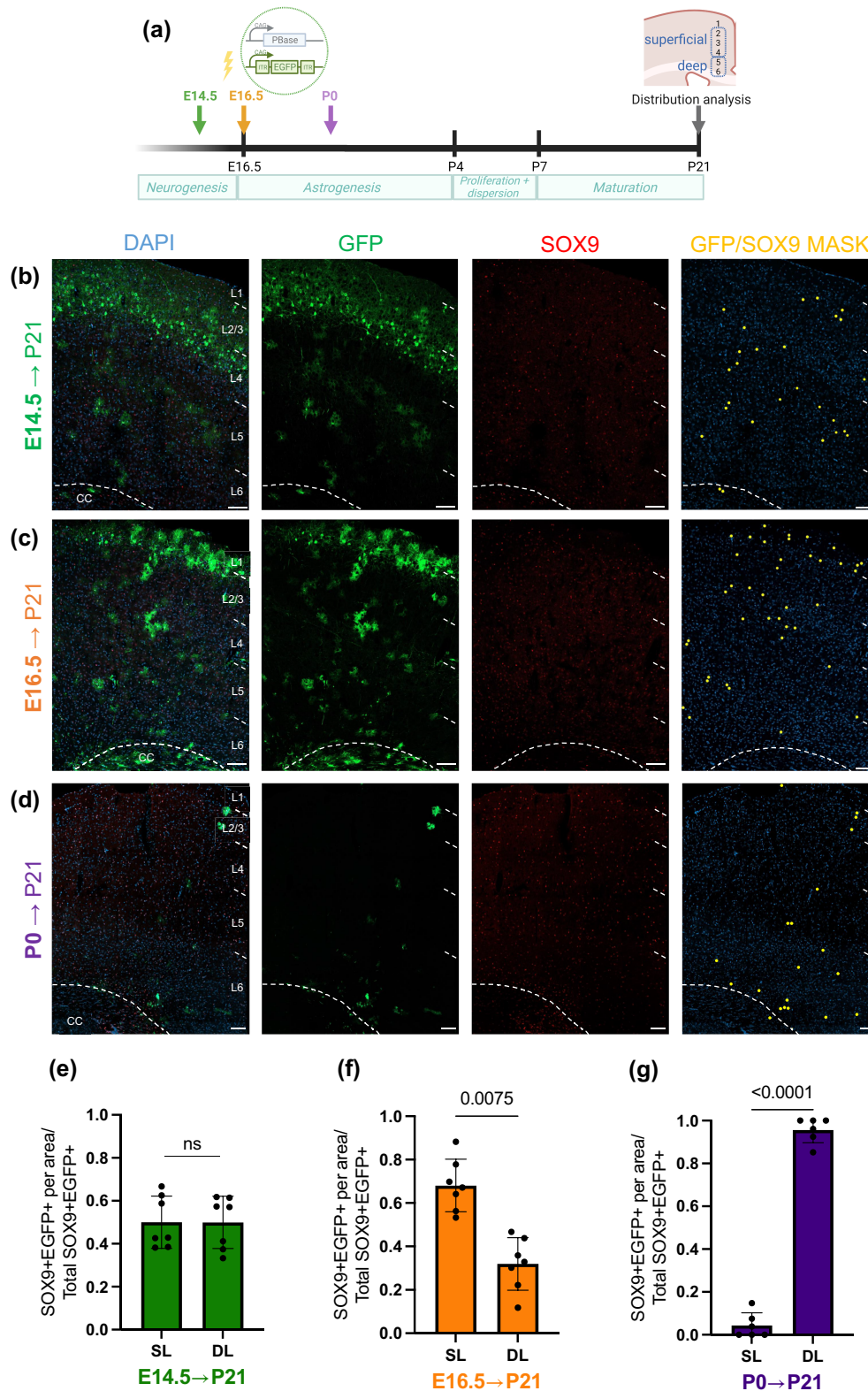
FIGURE 1 Legend on next page.

3.1.3 | E16.5- and P0-labeled astrocytes are molecularly and morphologically different

Given the layer biases of E16.5- and P0-born astrocytes, we then probed the molecular and morphological differences between astrocytes labeled at different times within the same cortical region (Figure 4a). To capture individual E16.5- and P0-labeled astrocyte transcriptomes from either the SL or DL, we used a spatially resolved single cell platform, called tissueDISCO (Scott et al., 2024). VZ/SVZ progenitors were electroporated with PB-CAG::EGFP at E16.5 and P0, time points where we had observed a biased distribution of astrocytes born from apical progenitors (Figure 3c,e). Fifteen E16.5-labeled and 28 P0-labeled EGFP+SOX9+ astrocytes were captured from the SL or DL at P21 using tissueDISCO for downstream scRNAseq (Scott et al., 2024). We detected 77 differentially expressed genes between E16.5 and P0 labeled cells. The top differentially expressed genes between E16.5- and P0-labeled astrocytes, irrespective of region include *Rplp2, Tecr, Trpm6, Alox8, Nsfl1c, Gm43660, Calm3, and Chpt1* (Figure 4b). Of these, a few genes showed further differences based on their location in the SL or DL (*Rplp2, Tecr Trmp6, Nsfl1c, Gm43660,* and *Rappget3*) (Figure 4b). These findings suggest that time drives molecular differences in cortical astrocytes with further differences based on their spatial localization within the cortex.

Next, we examined whether astrocytes in the same region labeled at different times would show morphological differences, a measure that may closely relate to astrocyte function (Endo et al., 2022). We first assessed the territorial volume of protoplasmic astrocytes from E16.5- and P0-*PB*-CAG::EGFP electroporated cortices. Analysis at P21 showed that E16.5-labeled astrocytes in layers 2/3 and layer 4 were larger than astrocytes in layers 5 and 6 (Figure 4c,d). Surprisingly, P0-labeled astrocytes showed no differences in territorial volume across the cortical layers (Figure 4c,d). When we compared E16.5- and P0-labeled astrocytes within each layer, we found that E16.5- and P0-labeled astrocytes were different in layers 2/3 and 4 (Figure 4d).

As astrocyte morphologies change as they mature (Clavreul et al., 2019), we asked if there would be a difference in territorial volumes across layers in E16.5- and P0-labeled astrocytes later in adulthood. When we compared astrocytes at P21 and P56, we observed larger volumes in E16.5-labeled astrocytes at P56 in layers 2/3, 4 and 5 but not layer 6, as expected (Figure 4d,e; One-way ANOVA, $p = .0001$, $F = 17.36$; E16.5 L2/3, $p < .0001$, E16.5 L4, $p = .0003$;

E16.5 L5, $p = .0009$). However, no differences were observed in P0-labeled astrocytes in any layer at P56 compared to P21 (Figure 4d,e). Analysis of astrocytes at P56 showed that E16.5-labeled cells in layers 2/3 were larger than cells in layers 4, 5, and 6 (Figure 4d). This is in line with a previous study of layer-specific morphological differences in astrocytes (Lanjakornsiripan et al., 2018). In P0-labeled cells, we found no differences, similar to our findings at P21. Lastly, when we compared E16.5- and P0-labeled astrocytes within each layer at P56, we found larger E16.5 labeled astrocytes in layers 2/3 (Figure 4e).

Since we observed time-dependent differences in territorial volume, we then performed a comprehensive characterization of the three-dimensional morphologies of E16.5- and P0-labeled cortical astrocytes. We imaged astrocytes from E16.5- and P0-labeled cortices at P21 or P56 across layers 1 to 6 (Video S1). As in a previous study (Lanjakornsiripan et al., 2018), we used an unbiased clustering analysis and identified seven clusters based on morphological features (Figure 4f). When we examined the proportion of cells within each cluster originating from E16.5- or P0-labeled astrocytes (Figure 4g), we found that cluster 7 was comprised of only E16.5 labeled astrocytes (Figure 4f). Strikingly, these cluster 7 cells were mostly comprised of layer 2/3 astrocytes (Figure S5a,b). We also found a high proportion of E16.5 labeled, layer 4 astrocytes in clusters 4 and 6 (Figure S5a,b) Of interest, cluster 4 morphologies were predominant at P21, while cluster 6 morphologies were predominant at P56, similar to our findings showing differences in territorial volume of layer 4 astrocytes at P21 and P56 (Figure 4e). Our analysis also showed that morphological features in clusters 1–5 were comprised of P0-labeled cells in all layers at both P21 and P56 (Figure 4g and Figure S5a,b). This suggests that E16.5-labeled astrocytes show different morphologies in different layers, while P0-labeled astrocytes are characterized by different morphologies that are present across all layers. Altogether, these data suggest that there is morphological and molecular diversity in astrocytes within the same local environment that depends on time of birth.

4 | DISCUSSION

In the cortex, protoplasmic astrocytes show layer-based differences in their molecular profiles and morphologies (Bayraktar et al., 2018; Lanjakornsiripan et al., 2018; Morel et al., 2017), but how these

FIGURE 1 *PiggyBac* fate mapping of ventricular/subventricular zone (VZ-SVZ) progenitor cells reveals time-dependent biases in the distribution of their astrocyte progeny within the superficial and deep cortical layers at P21. (a) Schematic of experimental design. VZ-SVZ progenitor cells were electroporated with PB-CAG::EGFP at E14.5, E16.5, or P0 and cortices were analyzed at P21. (b) Representative images show distribution of SOX9+ astrocytes in an E14.5 electroporated cortex at P21. Fourth panel shows distribution of EGFP+SOX9+ cells represented by yellow dots. Dotted lines show demarcation of cortical layers (L1, L2/3, L4, L5, L6) and corpus callosum (cc). Labeled in left most panel. Scale bar = 100 μm. (c) Representative images show distribution of SOX9+ astrocytes in an E16.5 electroporated cortex at P21. Fourth panel shows distribution of EGFP+SOX9+ cells represented by yellow dots. Dotted lines show demarcation of cortical layers (L1, L2/3, L4, L5, L6) and cc. Labeled in left most panel. Scale bar = 100 μm. (d) Representative images show distribution of SOX9+ astrocytes in a P0 electroporated cortex at P21. Fourth panel shows distribution of EGFP+SOX9+ cells represented by yellow dots. Dotted lines show demarcation of cortical layers (L1, L2/3, L4, L5, L6) and cc. Labeled in left most panel. Scale bar = 100 μm. (e) Quantification of E14.5-labeled EGFP+SOX9+ astrocytes at P21. (f) Quantification of E16.5-labeled EGFP+SOX9+ astrocytes at P21. (g) Quantification of P0-labeled EGFP+SOX9+ astrocytes at P21. DL, deep layers; SL, superficial layers. Source data are provided in Table S1.

regionally distinct astrocyte populations are established is not well understood. Here, we examined how "time of birth" influences the laminar position of protoplasmic astrocytes using a battery of fate mapping strategies. We showed that temporal patterning of neural progenitors is important for astrocyte localization in the SL and DL. Using morphological and molecular analyses we further show that E16.5- and P0-labeled astrocytes show distinct morphologies and gene expression signatures.
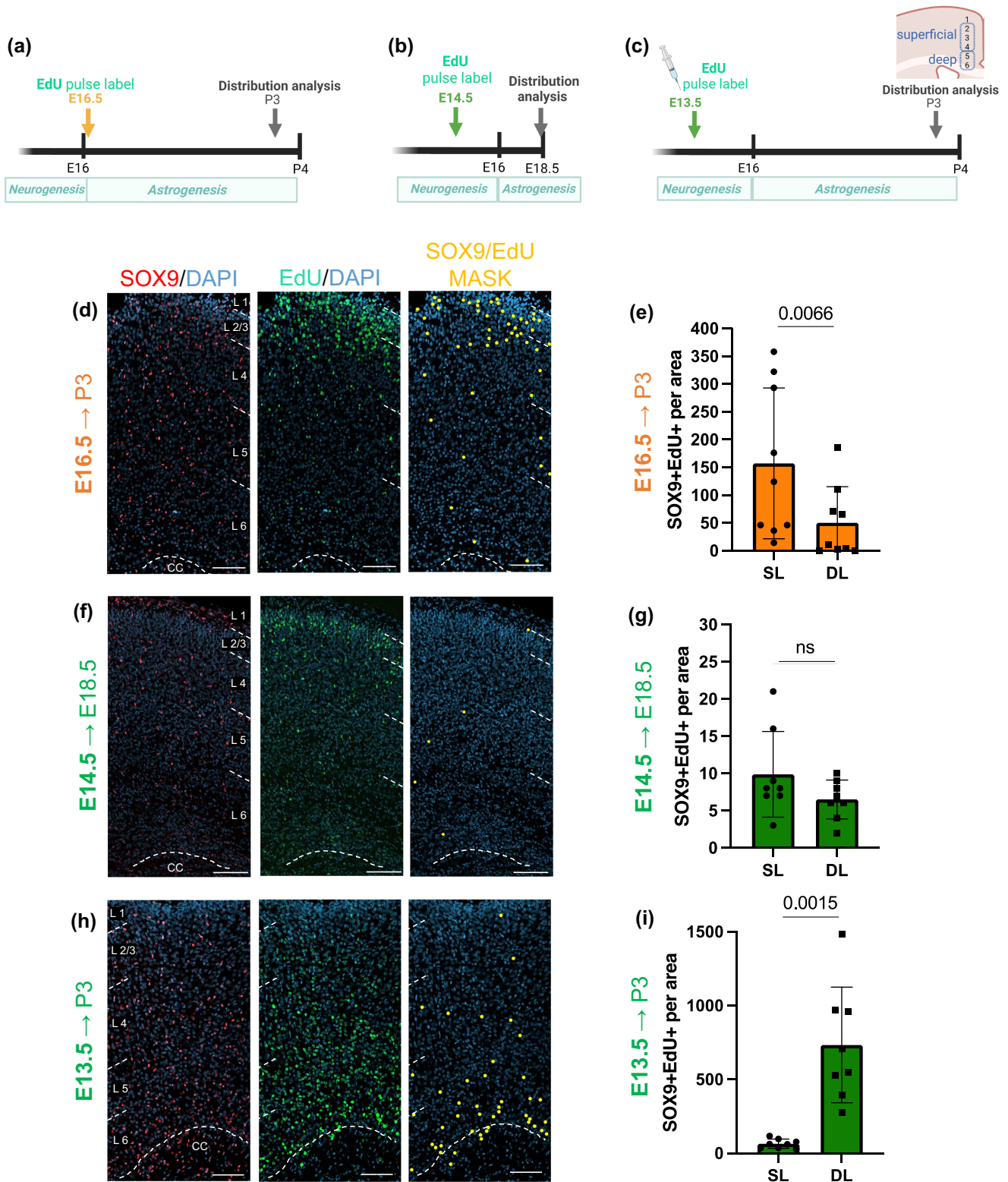

FIGURE 2 Legend on next page.

FIGURE 3 FlashTag (FT) labeling of apical progenitors shows time of birth influences the localization of astrocytes in the superficial and deep cortical layers. (a) Schematic of experimental design. FT pulse-labeling of apical radial progenitors (RP) was performed at E16.5 or P0 and cortices were analyzed at P3. (b) Representative images show distribution of SOX9+ astrocytes in a E16.5 FT pulse-labeled cortex at P3. Third panel shows distribution of FT+SOX9+ cells represented by yellow dots. Dotted lines show demarcation of cortical layers (L1, L2/3, L4, L5, L6) and corpus callosum (cc). Labeled in left most panel. Scale bar = 100 μm. (c) Quantification of E16.5-FT+SOX9+ astrocytes at P3. *p* value = .0001, *F* = 8.125. (d) Representative images show distribution of SOX9+ astrocytes in a P0 FT pulse-labeled cortex at P3. Third panel shows distribution of FT+SOX9+ cells represented by yellow dots. Dotted lines show demarcation of cortical layers (left) and cc. Scale bar = 100 μm. (e) Quantification of P0- FT+SOX9+ astrocytes at P3. *p* value = <.0001, *F* = 52.55. Cortical layer = L. Source data are provided in Table S1.
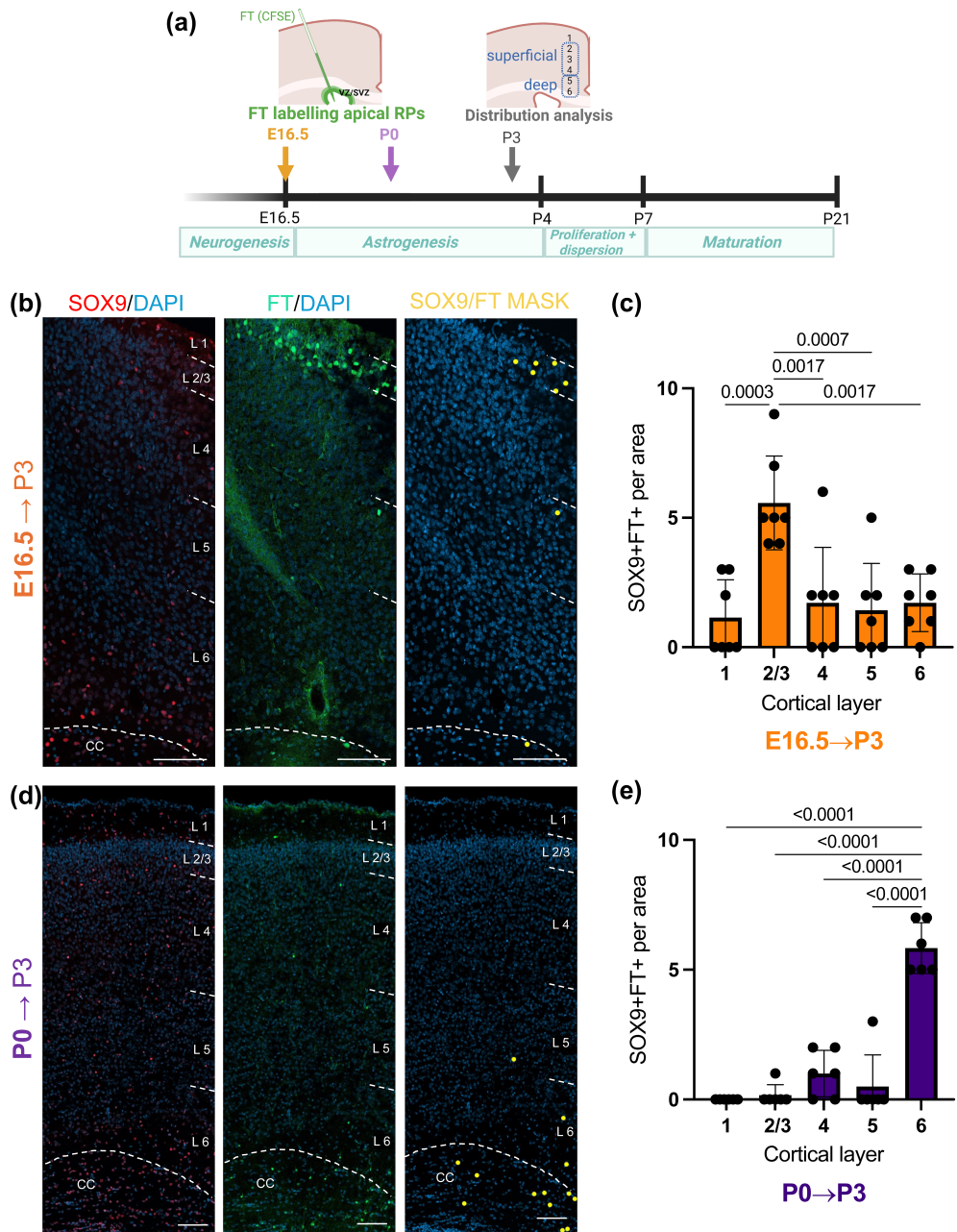
FIGURE 2 EdU fate mapping of cortical astrocytes at E16.5 and E13.5 shows a time-dependent bias in their distribution within superficial and deep layers at P3. (a) Schematic of experimental design. EdU pulse-labeling was performed at E16.5 and cortices were analyzed at P3. (b) Schematic of experimental design. EdU pulse-labeling was performed at E14.5, cortices were analyzed at E18.5. (c) Schematic of experimental design. EdU pulse-labeling was performed at E13.5, cortices were analyzed at P3. (d) Representative images show distribution of SOX9+ astrocytes in an E16.5 EdU pulse-labeled cortex at P3. Third panel shows distribution of EdU+SOX9+ cells represented by yellow dots. Dotted lines show demarcation of cortical layers (L1, L2/3, L4, L5, L6) and corpus callosum (cc). Labeled in left most panel. Scale bar = 100 μm. (e) Quantification of E16.5 labeled SOX9+EdU+ astrocytes at P3. (f) Representative images show distribution of SOX9+ astrocytes in a E14.5 EdU pulse-labeled cortex at E18.5. Third panel shows distribution of EdU+SOX9+ cells represented by yellow dots. Dotted lines show demarcation of cortical layers (L1, L2/3, L4, L5, L6) and cc. Labeled in left most panel. Scale bar = 100 μm. (g) Quantification of E14.5 labeled SOX9+EdU+ astrocytes at E18.5. (h) Representative images show distribution of SOX9+ astrocytes in a E13.5 EdU pulse-labeled cortex at P3. Third panel shows distribution of EdU+SOX9+ cells represented by yellow dots. Dotted lines show demarcation of cortical layers (L1, L2/3, L4, L5, L6) and cc. Labeled in left most panel. Scale bar = 100 μm. (i) Quantification of E13.5 labeled SOX9+EdU+ astrocytes at P3. DL, deep layers; SL, superficial layers. Cortical layer = L. Source data are provided in Table S1.
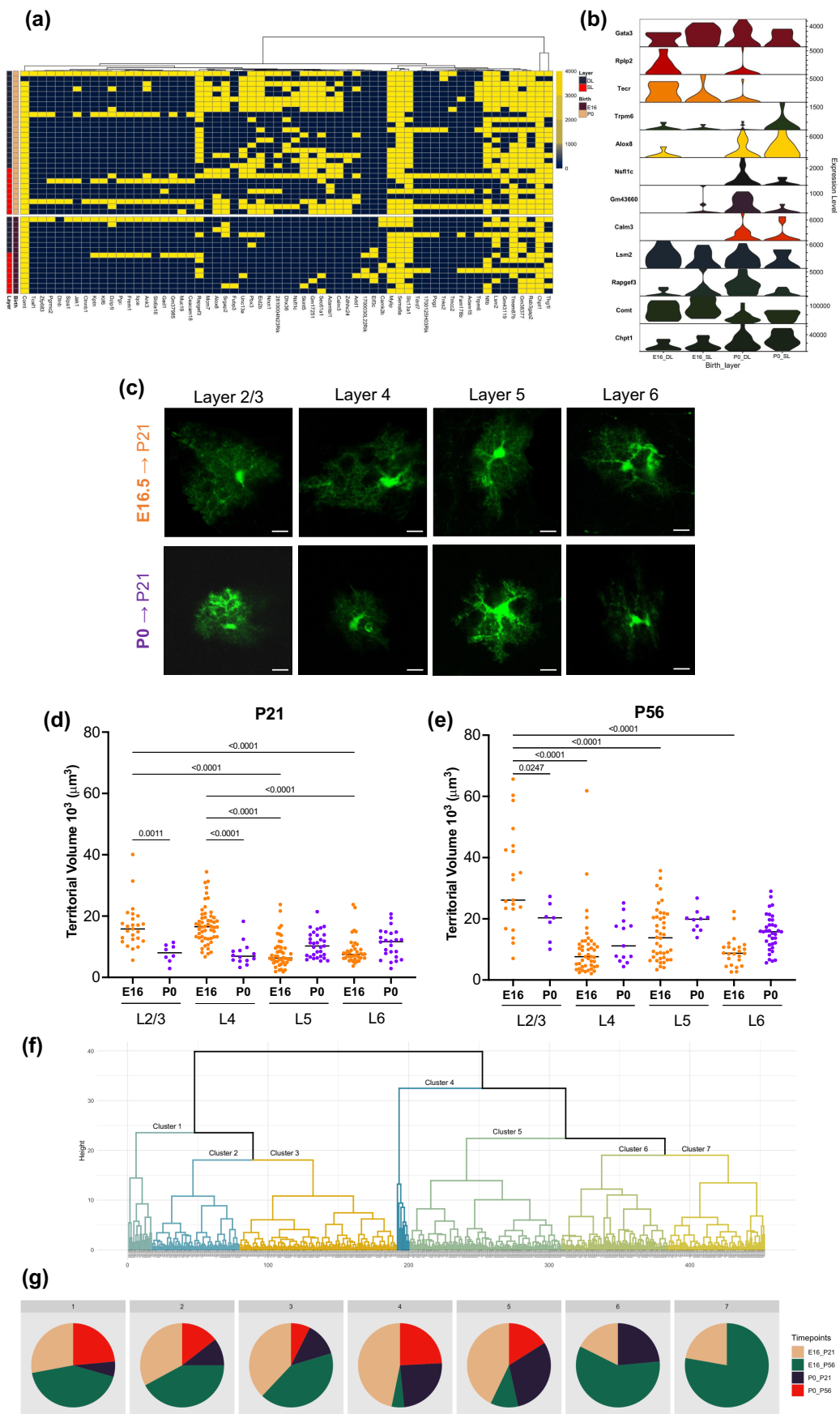
FIGURE 4 Legend on next page.

Altogether, our work contributes to understanding how cortical astrocytes are established in development. Early studies of astrocyte colonization of the cortex focused on the late embryonic and early postnatal period. This work established the production of astrocytes from radial glial cells and their progenitors in the VZ/SVZ (Li et al., 2021; Luskin & McDermott, 1994; Tabata, 2015), subpallial progenitors located in the ganglionic eminences (Marshall & Goldman, 2002), and Olig2-lineage cells (Dimou et al., 2008). However, correlation between time of birth and astrocyte distribution in the cortex was lacking. More recent studies have used MADM- and multifluorescent combinatorial labeling to understand how individual progenitors give rise to different protoplasmic (2–6) and pial astrocyte populations (layer 1) and their ultimate positions in the cortex (Clavreul et al., 2019; Gao et al., 2014; Garcia-Marques & Lopez-Mascaraque, 2013). MADM showed the production of astrocytes in radial units, while Star Track and Clone showed a wider distribution of clones throughout the cortex. Nonetheless, in these studies, progenitors were labeled at a single time point (either E14.5 or E15.5), with no analysis of the effect of time.

The focus of our study was understanding how time influences astrogenesis from pallial VZ/SVZ progenitors. Our approach involved the comparison of SL and DL astrocytes by grouping layers 2–4 (SL) and layers 5–6 (DL), based on previously defined differences in their molecular and morphological profiles (Bayraktar et al., 2018; Lanjakornsiripan et al., 2018; Morel et al., 2017). Using *PB*-CAG-EGFP electroporation and EdU labeling, we found a biased production of SL astrocytes in late embryogenesis (E15.5–E17.5), while DL astrocytes were mainly produced after birth (P0–P7). When we investigated the contribution of apical progenitors to this layer bias in astrocytes using FT, we found a similar bias of E16.5-born astrocytes in the SL and P0-born astrocytes in the DL. When we further examined FT+ astrocyte localization within each cortical layer, we found that apical progenitors labeled at E16.5 gave rise to astrocytes in layers 2/3 while progenitors labeled at P0- gave rise to astrocytes in layer 6. These findings may reflect the production of astrocytes directly from apical progenitors; SL and DL biases could be due to the somal translocation of apical progenitors in late embryogenesis (Clavreul et al., 2019) and retraction of their pial processes in the early postnatal period (Noctor et al., 2008).

A novel finding is that the production of astrocytes follows the developmental timing of neurons. With EdU fate mapping, which is progenitor cell type agnostic, we found that astrocytes born from E16.5-labeled progenitors (during late neurogenesis) distribute in the SL, corresponding to the production of SL neurons at this time (Berry & Rogers, 1965). Similarly, at E13.5 (during early neurogenesis), we found a DL astrocyte bias, in line with DL neurons produced at this time.

Of interest, FT labeling at E13.5 did not reveal a DL bias, which may suggest that E13.5-born astrocytes are from a distinct progenitor pool. In addition to pallial progenitors, cortical astrocytes derive from NG2+ glia and subpallial progenitors (Sanchez-Gonzalez et al., 2020). Both Olig2+ (Clavreul et al., 2019; Tatsumi et al., 2018) and Gli1+ (Gingrich et al., 2022) progenitors have been shown to disperse prenatally in the cortical parenchyma and give rise to protoplasmic astrocytes (Ojalvo-Sanz & Lopez-Mascaraque, 2021). Similarly, our data suggests that E14.5-labeled astrocytes may derive from a subset of fast-dividing progenitors, given that we could detect SOX9+ astrocytes at E18.5 but not P3. As we see no bias in E14.5-labeled astrocytes, it is also interesting to speculate that a subset of progenitors (set aside) at E14.5 can generate both SL and DL astrocytes throughout astrogenesis.

In this study, we examined the morphology of astrocytes at P21 and P56 as it relates to time of birth. When we examined territorial volumes, we found that E16.5-labeled astrocytes are approximately 10,100 μm^3, while P0-labeled astrocytes are 7500 μm^3 at P21. By P56, the average volume increased to 17,300 μm^3 and 16,800 μm^3 for E16.5- and P0-labeled astrocytes, respectively. This increase is consistent with astrocyte maturation during this period, but these volumes differ from those reported in other studies (Clavreul et al., 2019; Lanjakornsiripan et al., 2018; Oberheim et al., 2009). Oberheim et al. reported volumes of adult mouse astrocytes as 6000 μm^3 (Oberheim et al., 2009), in Clavreul et al. P21 astrocytes were 75,000 μm^3 (Clavreul et al., 2019), while Lanjakornsiripan et al. showed an average volume of P60 mouse astrocytes of approximately 100,000 μm^3, with further variation between layers (Lanjakornsiripan et al., 2018). Different methodological approaches (tissue clearing, transgenic reporters versus *in utero* electroporation) could account for some of these differences. These differences could also be explained by heterogeneity within the astrocyte population. Our study of E16.5- and P0-born astrocytes could represent a small subpopulation of cells within the total astrocyte pool. In support of this, a recent study

FIGURE 4 E16.5 and P0-*PiggyBac* labeled astrocytes show differences in gene expression and morphology. (a) The heatmap represents 77 hierarchically clustered DEGs (general linear model with contrasts, FDR <0.05, columns) between E16.5- and P0-labeled cells (rows), which are color-coded according to superficial layer (SL, red) versus deep layer (DL, blue) and time (E16.5, maroon; P0, beige). (b) The violin plot shows gene expression (log-normalized, y-axis) of DEGs identified from tDISCO analysis in (a) in SL and DL astrocytes from E16- and P0-labeled cells. (c) Representative images of E16.5- and P0-labeled EGFP+ astrocytes in each cortical layer analyzed. Scale bar = 5 μm. (d) Quantification of territorial volume from P21 astrocytes labeled at E16.5 and P0. Only significant comparisons of cortical layers within E16.5- or P0-labeled groups and of E16.5- and P0-labeled astrocytes within each layer are shown. p value = <.0001, F = 18.71. (e) Quantification of territorial volume from P56 astrocytes labeled at E16.5 and P0. Only significant comparisons of cortical layers within E16.5- or P0-labeled groups and of E16.5- and P0-labeled astrocytes within each layer are shown. p value = <.0001, F = 14.78. (f) Hierarchical clustered dendrogram (using Ward 2 criterion) shows that astrocytes can be separated into 7 clusters (color-coded and formed after cutting at a height of 15). Each branch (value on x-axis) represents a different cell from E16.5- and P0-labeled brains captured at P21 or P56. (g) Pie charts show the proportion of astrocytes in each cluster (1–7) labeled at E16.5 or P0 and captured at P21 or P56. Source data are provided in Table S2.

shows smaller clone size in spatially restricted versus nonrestricted clones at P30 following labeling of pallial progenitors at E12.5, E14.5, and E16.5 (Ojalvo-Sanz et al., 2024). Morphological measurements that sample the entire astrocyte population (as in Lanjakornsiripan et al., 2018) could be biased toward the most abundant astrocyte type(s).

Of interest, our data showed morphological diversity related to time of birth. While E16.5-labeled astrocytes showed that layer 2/3 astrocytes were larger than 5/6 astrocytes, similar to previous studies (Lanjakornsiripan et al., 2018), no differences were found in the volumes of P0-labeled astrocytes. Clustering analysis also showed that E16.5- and P0-labeled progenitors give rise to morphologically diverse astrocyte populations within the same region. Of interest, considerable variability in the territorial volume and types of morphologies within different layers was seen, as in Lanjakornsiripan et al. (2018). This may suggest further diversification of E16.5- and P0-labeled astrocytes within specific regions when exposed to different local environments.

A changing environment that relates to ongoing developmental processes, including neurogenesis and angiogenesis, could also influence astrocyte heterogeneity. Previous studies have shown that blood vessels are involved in cortical astrocyte specification and their distribution within the cortex (Molofsky et al., 2012; Tabata et al., 2022; Zerlin & Goldman, 1997). Similarly, the transcriptional diversity of cortical astrocytes that is observed in SL and DL astrocytes is influenced by neuronal factors. Altered gene expression in SL astrocytes was observed in *Satb2* conditional knockout mice and SL and DL astrocyte signatures were inverted in *Reelin* mice (Bayraktar et al., 2018). In our study, we analyzed astrocytes in SL and DL but time of label was used as an additional selection criterion. When we compared E16.5- and P0-labeled astrocytes in SL and DL, we primarily found differential gene expression based on time. In P0-labeled cells, we found enriched expression of *Calm3*. *Calm3* was previously shown to increase in response to the oligodendrocyte secretome, which may be more available in the postnatal period due to ongoing oligodendrogenesis (Iacobas et al., 2020). In E16-labeled cells, we found upregulation of the *Comt*, a gene known to be predominantly expressed in astrocytes alongside Maob, and important for dopamine metabolism (Petrelli et al., 2020). Interestingly we also found enrichment of the gene *Tecr*, which is associated with blood brain barrier maturation and with vascular sprouting (Wang et al., 2022). While gene expression differences could result from differences in local signals, environmental cues within the SL and DL may not be the only factors influencing astrocyte diversity. The relative contribution of intrinsic and extrinsic cues remains to be determined.

An intriguing idea is that the timed production of astrocytes from distinct progenitor pools could also contribute to their transcriptional diversity. This could also be important for ongoing developmental processes (Zerlin & Goldman, 1997). Indeed, subpallial progenitors show enrichment in *Sparcl1*, which may suggest a more specialized role in synapse regulation (Liu et al., 2022). A recent preprint using computational analysis of developmental datasets suggests that molecularly diverse astrocytes are produced from at least two different progenitor pools (*Emx1*- and *Olig2*- lineages) (Zhou et al., 2023). Within the *Emx1*-lineage, two transcriptomically distinct astrocyte states were found with different laminar distributions. Whether these *Emx1*-lineage astrocyte populations correspond to E16.5- and P0-labeled astrocytes is an interesting future question.

Finally, there are three main caveats of this study. First, our analysis of EdU and FT fate labeling was performed at P3, prior to the period of astrocyte expansion and migration, due to label dilution. Therefore, we are unable to examine differences in the dispersion in timed subsets of SL and DL astrocytes, which may also be important. As a result, our conclusions from these experiments are limited to the influence of time of birth on the "seeding" of astrocytes in the cortex. Second, astrocytes were selected using tissueDISCO in PFA-fixed sections, using custom new methodologies developed for this purpose. It is well known that PFA fixation can degrade RNA quality (Evers et al., 2011), so it is not surprising that most of the genes that were detected in this analysis were highly expressed. Moreover, tissueDISCO is a precise technique that is well suited for selective profiling of a targeted subpopulation of cells, but it is not applicable for broad analysis of an entire tissue section. Therefore, it is possible that future analysis using spatial -Omics methods that interrogate entire tissue sections (but with limited cell-by-cell precision) may help identify more extensive transcriptomic differences between E16.5- and P0-labeled astrocyte populations. Third, SOX9 was used to quantify astrocytes in the P3 cortex. *Sox9* is a transcription factor that plays a crucial role in determining astrocyte lineage and is used as a marker for astrocytes and their progenitors (Stolt et al., 2003). Nonetheless, SOX9 does not represent the entire population of astrocytes in the cortex, and its expression in mature astrocytes increases significantly at 1 month of age in mice (Sun et al., 2017). Therefore, quantification of astrocyte distribution in SL and DL as new markers become available that can identify the spectrum of astrocyte lineage cell types will be of interest. These studies will lead to a more comprehensive understanding of if/how the timed generation of diverse astrocyte populations from progenitor cells contributes to the colonization of the cortex.

In summary, this study adds to the existing framework of cortical astrocyte development to show that, akin to neurons, timing is an important factor in the production of different (SL and DL) astrocyte populations. Further work that identifies the intrinsic and extrinsic mechanisms that result in the spatial, morphological, and molecular diversity of cortical astrocytes and how this relates to astrocyte function will be an exciting area for a future study.

AUTHOR CONTRIBUTIONS

CONFLICT OF INTEREST STATEMENT

The authors declare no competing interests.

DATA AVAILABILITY STATEMENT

The source data that supports the findings of this study are provided in Tables S1 and S2.

ORCID

Daniela Lozano Casasbuenas https://orcid.org/0000-0002-7475-672X

Patrick Küry https://orcid.org/0000-0002-2654-1126

Aaron R. Wheeler https://orcid.org/0000-0001-5230-7475

Martin Lévesque https://orcid.org/0000-0002-1547-3746

Maryam Faiz https://orcid.org/0000-0003-0671-3557

REFERENCES

Bandler, R. C., Vitali, I., Delgado, R. N., Ho, M. C., Dvoretskova, E., Ibarra Molinas, J. S., Frazel, P. W., Mohammadkhani, M., Machold, R., Maedler, S., Liddelow, S. A., Nowakowski, T. J., Fishell, G., & Mayer, C. (2022). Single-cell delineation of lineage and genetic identity in the mouse brain. *Nature*, 601(7893), 404–409.

Bayraktar, O. A., Bartels, T., Polioudakis, D., Holmqvist, S., Ben Haim, L., Young, A. M. H., Prakash, K., Brown, A., Paredes, M. F., Kawaguchi, R., Stockley, J., Sabeur, K., Chang, S. M., Huang, E., Hutchinson, P., Ullian, E. M., Geschwind, D. H., Coppola, G., & Rowitch, D. H. (2018). Single-cell in situ transcriptomic map of astrocyte cortical layer diversity. *bioRxiv*.

Bayraktar, O. A., Fuentealba, L. C., Alvarez-Buylla, A., & Rowitch, D. H. (2014). Astrocyte development and heterogeneity. *Cold Spring Harbor Perspectives in Biology*, 7(1), a020362.

Berry, M., & Rogers, A. W. (1965). The migration of neuroblasts in the developing cerebral cortex. *Journal of Anatomy*, 99(Pt 4), 691–709.

Cerrato, V., Parmigiani, E., Figueres-Oñate, M., Betizeau, M., Aprato, J., Nanavaty, I., Berchialla, P., Luzzati, F., de'Sperati, C., López-Mascaraque, L., & Buffo, A. (2018). Multiple origins and modularity in the spatiotemporal emergence of cerebellar astrocyte heterogeneity. *PLoS Biology*, 16(9), e2005513.

Clavreul, S., Abdeladim, L., Hernández-Garzón, E., Niculescu, D., Durand, J., Ieng, S. H., Barry, R., Bonvento, G., Beaurepaire, E., Livet, J., & Loulier, K. (2019). Cortical astrocytes develop in a plastic manner at both clonal and cellular levels. *Nature Communications*, 10(1), 4884.

Dimou, L., Simon, C., Kirchhoff, F., Takebayashi, H., & Götz, M. (2008). Progeny of Olig2-expressing progenitors in the gray and white matter of the adult mouse cerebral cortex. *The Journal of Neuroscience*, 28(41), 10434–10442.

Endo, F., Kasai, A., Soto, J. S., Yu, X., Qu, Z., Hashimoto, H., Gradinaru, V., Kawaguchi, R., & Khakh, B. S. (2022). Molecular basis of astrocyte diversity and morphology across the CNS in health and disease. *Science*, 378(6619), eadc9020.

Evers, D. L., Fowler, C. B., Cunningham, B. R., Mason, J. T., & O'Leary, T. J. (2011). The effect of formaldehyde fixation on RNA: Optimization of formaldehyde adduct removal. *The Journal of Molecular Diagnostics*, 13(3), 282–288.

Fuentealba, L. C., Rompani, S. B., Parraguez, J. I., Obernier, K., Romero, R., Cepko, C. L., & Alvarez-Buylla, A. (2015). Embryonic origin of postnatal neural stem cells. *Cell*, 161(7), 1644–1655.

Furutachi, S., Miya, H., Watanabe, T., Kawai, H., Yamasaki, N., Harada, Y., Imayoshi, I., Nelson, M., Nakayama, K. I., Hirabayashi, Y., & Gotoh, Y. (2015). Slowly dividing neural progenitors are an embryonic origin of adult neural stem cells. *Nature Neuroscience*, 18(5), 657–665.

Gao, P., Postiglione, M. P., Krieger, T. G., Hernandez, L., Wang, C., Han, Z., Streicher, C., Papusheva, E., Insolera, R., Chugh, K., Kodish, O., Huang, K., Simons, B. D., Luo, L., Hippenmeyer, S., & Shi, S. H. (2014). Deterministic progenitor behavior and unitary production of neurons in the neocortex. *Cell*, 159(4), 775–788.

Garcia-Marques, J., & Lopez-Mascaraque, L. (2013). Clonal identity determines astrocyte cortical heterogeneity. *Cerebral Cortex*, 23(6), 1463–1472.

Ge, W. P., Miyawaki, A., Gage, F. H., Jan, Y. N., & Jan, L. Y. (2012). Local generation of glia is a major astrocyte source in postnatal cortex. *Nature*, 484(7394), 376–380.

Gingrich, E. C., Case, K., & Garcia, A. D. R. (2022). A subpopulation of astrocyte progenitors defined by sonic hedgehog signaling. *Neural Development*, 17(1), 2.

Govindan, S., Oberst, P., & Jabaudon, D. (2018). In vivo pulse labeling of isochronic cohorts of cells in the central nervous system using Flash-Tag. *Nature Protocols*, 13(10), 2297–2311.

Guillemot, F. (2007). Spatial and temporal specification of neural fates by transcription factor codes. *Development*, 134(21), 3771–3780.

Hochstim, C., Deneen, B., Lukaszewicz, A., Zhou, Q., & Anderson, D. J. (2008). Identification of positionally distinct astrocyte subtypes whose identities are specified by a homeodomain code. *Cell*, 133(3), 510–522.

Hofer, T., Busch, K., Klapproth, K., & Rodewald, H.-R. (2016). Fate mapping and quantitation of hematopoiesis in vivo. *Annual Review of Immunology*, 34, 449–478.

Huang, W., Zhao, N., Bai, X., Karram, K., Trotter, J., Goebbels, S., Scheller, A., & Kirchhoff, F. (2014). Novel NG2-CreERT2 knock-in mice demonstrate heterogeneous differentiation potential of NG2 glia during development. *Glia*, 62(6), 896–913.

Iacobas, D. A., Iacobas, S., Stout, R. F., & Spray, D. C. (2020). Cellular environment remodels the genomic fabrics of functional pathways in astrocytes. *Genes*, 11(5), 520.

Lanjakornsiripan, D., Pior, B. J., Kawaguchi, D., Furutachi, S., Tahara, T., Katsuyama, Y., Suzuki, Y., Fukazawa, Y., & Gotoh, Y. (2018). Layer-specific morphological and molecular differences in neocortical astrocytes and their dependence on neuronal layers. *Nature Communications*, 9(1), 1623.

Li, X., Liu, G., Yang, L., Li, Z., Zhang, Z., Xu, Z., Cai, Y., du, H., Su, Z., Wang, Z., Duan, Y., Chen, H., Shang, Z., You, Y., Zhang, Q., He, M., Chen, B., & Yang, Z. (2021). Decoding Cortical Glial Cell Development. *Neuroscience Bulletin*, 37(4), 440–460.

Liu, J., Wu, X., & Lu, Q. (2022). Molecular divergence of mammalian astrocyte progenitor cells at early gliogenesis. *Development*, *149*(5), dev199985.

Luskin, M. B., & McDermott, K. (1994). Divergent lineages for oligodendrocytes and astrocytes originating in the neonatal forebrain subventricular zone. *Glia*, *11*(3), 211–226.

Magavi, S., Friedmann, D., Banks, G., Stolfi, A., & Lois, C. (2012). Coincident generation of pyramidal neurons and protoplasmic astrocytes in neocortical columns. *The Journal of Neuroscience*, *32*(14), 4762–4772.

Marshall, C. A., & Goldman, J. E. (2002). Subpallial dlx2-expressing cells give rise to astrocytes and oligodendrocytes in the cerebral cortex and white matter. *The Journal of Neuroscience*, *22*(22), 9821–9830.

Miller, F. D., & Gauthier, A. S. (2007). Timing is everything: Making neurons versus glia in the developing cortex. *Neuron*, *54*(3), 357–369.

Molofsky, A. V., Krenick, R., Ullian, E., Tsai, H. H., Deneen, B., Richardson, W. D., Barres, B. A., & Rowitch, D. H. (2012). Astrocytes and disease: A neurodevelopmental perspective. *Genes & Development*, *26*(9), 891–907.

Molyneaux, B. J., Arlotta, P., Menezes, J. R. L., & Macklis, J. D. (2007). Neuronal subtype specification in the cerebral cortex. *Nature Reviews. Neuroscience*, *8*(6), 427–437.

Morel, L., Chiang, M. S. R., Higashimori, H., Shoneye, T., Iyer, L. K., Yelick, J., Tai, A., & Yang, Y. (2017). Molecular and functional properties of regional astrocytes in the adult brain. *The Journal of Neuroscience*, *37*(36), 8706–8717.

Nery, S., Fishell, G., & Corbin, J. G. (2002). The caudal ganglionic eminence is a source of distinct cortical and subcortical cell populations. *Nature Neuroscience*, *5*(12), 1279–1287.

Noctor, S. C., Martinez-Cerdeno, V., & Kriegstein, A. R. (2008). Distinct behaviors of neural stem and progenitor cells underlie cortical neurogenesis. *The Journal of Comparative Neurology*, *508*(1), 28–44.

Oberheim, N. A., Takano, T., Han, X., He, W., Lin, J. H. C., Wang, F., Xu, Q., Wyatt, J. D., Pilcher, W., Ojemann, J. G., Ransom, B. R., Goldman, S. A., & Nedergaard, M. (2009). Uniquely hominid features of adult human astrocytes. *The Journal of Neuroscience*, *29*(10), 3276–3287.

Oberst, P., Fièvre, S., Baumann, N., Concetti, C., Bartolini, G., & Jabaudon, D. (2019). Temporal plasticity of apical progenitors in the developing mouse neocortex. *Nature*, *573*(7774), 370–374.

Ojalvo-Sanz, A. C., & Lopez-Mascaraque, L. (2021). Gliogenic potential of single pallial radial glial cells in lower cortical layers. *Cells*, *10*(11), 3237.

Ojalvo-Sanz, A. C., Pernia-Solanilla, C., & Lopez-Mascaraque, L. (2024). Spatial organization of astrocyte clones: The role of developmental progenitor timing. *Glia*, *72*, 1290–1303.

Ollion, J., Cochennec, J., Loll, F., Escudé, C., & Boudier, T. (2013). TANGO: A generic tool for high-throughput 3D image analysis for studying nuclear organization. *Bioinformatics*, *29*(14), 1840–1841.

Petrelli, F., Dallérac, G., Pucci, L., Calì, C., Zehnder, T., Sultan, S., Lecca, S., Chicca, A., Ivanov, A., Asensio, C. S., Gundersen, V., Toni, N., Knott, G. W., Magara, F., Gertsch, J., Kirchhoff, F., Déglon, N., Giros, B., Edwards, R. H., … Bezzi, P. (2020). Dysfunction of homeostatic control of dopamine by astrocytes in the developing prefrontal cortex leads to cognitive impairments. *Molecular Psychiatry*, *25*(4), 732–749.

Sanchez-Gonzalez, R., Bribian, A., & Lopez-Mascaraque, L. (2020). Cell fate potential of NG2 progenitors. *Scientific Reports*, *10*(1), 9876.

Scott, E. Y., Safarian, N., Casasbuenas, D. L., Dryden, M., Tockovska, T., Ali, S., Peng, J., Daniele, E., Nie Xin Lim, I., Bang, K. W. A., Tripathy, S., Yuzwa, S. A., Wheeler, A. R., & Faiz, M. (2024). Integrating single-cell and spatially resolved transcriptomic strategies to survey the astrocyte response to stroke in male mice. *Nature Communications*, *15*(1), 1584.

Stolt, C. C., Lommes, P., Sock, E., Chaboissier, M. C., Schedl, A., & Wegner, M. (2003). The Sox9 transcription factor determines glial fate choice in the developing spinal cord. *Genes & Development*, *17*(13), 1677–1689.

Sun, W., Cornwell, A., Li, J., Peng, S., Osorio, M. J., Aalling, N., Wang, S., Benraiss, A., Lou, N., Goldman, S. A., & Nedergaard, M. (2017). SOX9 is an astrocyte-specific nuclear marker in the adult brain outside the neurogenic regions. *The Journal of Neuroscience*, *37*(17), 4493–4507.

Tabata, H. (2015). Diverse subtypes of astrocytes and their development during corticogenesis. *Frontiers in Neuroscience*, *9*, 114.

Tabata, H., & Nakajima, K. (2001). Efficient in utero gene transfer system to the developing mouse brain using electroporation: Visualization of neuronal migration in the developing cortex. *Neuroscience*, *103*(4), 865–872.

Tabata, H., Sasaki, M., Agetsuma, M., Sano, H., Hirota, Y., Miyajima, M., Hayashi, K., Honda, T., Nishikawa, M., Inaguma, Y., Ito, H., Takebayashi, H., Ema, M., Ikenaka, K., Nabekura, J., Nagata, K. I., & Nakajima, K. (2022). Erratic and blood vessel-guided migration of astrocyte progenitors in the cerebral cortex. *Nature Communications*, *13*(1), 6571.

Tatsumi, K., Isonishi, A., Yamasaki, M., Kawabe, Y., Morita-Takemura, S., Nakahara, K., Terada, Y., Shinjo, T., Okuda, H., Tanaka, T., & Wanaka, A. (2018). Olig2-lineage astrocytes: A distinct subtype of astrocytes that differs from GFAP astrocytes. *Frontiers in Neuroanatomy*, *12*, 8.

Tsai, H. H., Li, H., Fuentealba, L. C., Molofsky, A. V., Taveira-Marques, R., Zhuang, H., Tenney, A., Murnen, A. T., Fancy, S. P., Merkle, F., Kessaris, N., Alvarez-Buylla, A., Richardson, W. D., & Rowitch, D. H. (2012). Regional astrocyte allocation regulates CNS synaptogenesis and repair. *Science*, *337*(6092), 358–362.

Wang, J., Xu, J., Zang, G., Zhang, T., Wu, Q., Zhang, H., Chen, Y., Wang, Y., Qin, W., Zhao, S., Qin, E., Qiu, J., Zhang, X., Wen, L., Wang, Y., & Wang, G. (2022). Trans-2-enoyl-CoA reductase Tecr-driven lipid metabolism in endothelial cells protects against transcytosis to maintain blood-brain barrier homeostasis. *Research (Wash D C)*, *2022*, 9839368.

Zerlin, M., & Goldman, J. E. (1997). Interactions between glial progenitors and blood vessels during early postnatal corticogenesis: Blood vessel contact represents an early stage of astrocyte differentiation. *The Journal of Comparative Neurology*, *387*(4), 537–546.

Zhou, J., Vitalia, I., Roig-Puiggros, S., Javed, A., Jaboudon, D., Mayer, C., & Bocchi, R. (2023). Dual lineage origins of neocortical astrocytes. *bioRxiv*.

SUPPORTING INFORMATION

Additional supporting information can be found online in the Supporting Information section at the end of this article.